ELSEVIER

Physica D 138 (2000) 91–113

PHYSICA D

www.elsevier.com/locate/physd

Nonlinear doubly diffusive convection in vertical enclosures

G. Bardan [a,*], A. Bergeon [a], E. Knobloch [b], A. Mojtabi [a]

[a] *UMR 5502 IMFT-CNRS-UPS, UFR MIG, Université Paul Sabatier, 118, route de Narbonne, 31062 Toulouse Cedex, France*

[b] *Department of Physics, University of California, Berkeley, CA 94720, USA*

Received 24 March 1999; received in revised form 28 August 1999; accepted 11 September 1999

Communicated by S. Fauve

Abstract

Nonlinear doubly diffusive convection in two-dimensional enclosures driven by lateral temperature and concentration differences is studied using a combination of analytical and numerical techniques. The study is organized around a special case that allows a static equilibrium. The stationary states that bifurcate from this equilibrium are either symmetric or antisymmetric with respect to diagonal reflection. Local bifurcation analysis around the critical aspect ratio at which both modes appear simultaneously is complemented using numerical continuation. Perturbation of this situation to one in which no static equilibrium exists provides important information about the multiplicity of steady states in this system.

Keywords: Doubly diffusive convection; Nonlinear analysis; Mode interaction

1. Introduction

Doubly diffusive convection is of fundamental importance in many industrial applications as well as in geophysical flows [1–4]. Such flows are the result of diffusive instabilities that depend for their existence on the presence of two scalar fields (usually temperature T and concentration C) with different diffusivities, and occur when these contribute to the fluid buoyancy in opposite ways. For such states the buoyancy ratio $N < 0$, where $N \equiv \beta_C \Delta C / \beta_T \Delta T$, ΔT and ΔC are the temperature and concentration differences imposed across the fluid, and $\beta_{T,C} \equiv \partial\rho/\partial(T, C)$ are the corresponding expansion coefficients. The resulting flows can take the form of fingers or overstable motions such as traveling waves, all of which have been observed in experiments. These observations which have motivated a number of theoretical and numerical studies of doubly diffusive instabilities and their nonlinear development, and doubly diffusive convection is now considered a paradigm in the study of dynamical systems [5].

In this paper we study doubly diffusive flows driven by imposed *horizontal* temperature *and* concentration gradients, focusing on the interesting case $N < 0$. This situation is different from the cases usually considered, either imposed vertical gradients [6,7] or a stably stratified fluid cavity heated from the side [8–10]. In the latter

* Corresponding author. Tel.: +33-0-5-61-55-67-88; fax: +33-0-5-61-55-83-26.
E-mail address: bardan@imft.fr (G. Bardan).

0167-2789/00/$ – see front matter
PII: S0167-2789(99)00195-5

situation the imposed concentration and temperature gradients are orthogonal and no motion-free equilibrium is possible. This situation differs from that considered here in which the two imposed gradients are parallel, albeit horizontal. In this situation a motion-free equilibrium exists provided $N = -1$. This is no longer so when $N \neq -1$ and in this case experiments in small cavities and numerical simulations both indicate that the preferred sense of motion depends on the sign of $Le - 1$. Here the Lewis number Le is the ratio of the thermal and solutal diffusivities. However, the comparison between the experimental and numerical results remains qualitative rather than quantitative. One of the reasons is that when $Le \approx 100$ both unicellular and multicellular states can be observed in the range $-10 < N < 10$ [11–17], depending on the values of the thermal and solutal Rayleigh numbers [15]. In addition, the observed states may be steady or time-dependent. These observations which have been corroborated by the numerical simulations of Bennacer and Gobin [18] and Gobin and Bennacer [19] are furthermore sensitive to the value of the Schmidt number (kinematic viscosity divided by the solutal diffusivity) [12,15–17]. Turner [1] summarizes the dependence of the observed state on the values of the thermal and solutal Rayleigh numbers for large Lewis numbers when $N \neq -1$. The possible mechanisms responsible for the observed time dependence have been discussed by Chang and Lin [20], and Alavyoon [21].

In this paper we combine numerical continuation techniques with bifurcation theory to analyze in the first instance the states that develop from the instability of the conduction state when $N = -1$ and then investigate the behavior of the system for nearby values of N with a view to understand the multiplicity of states in this system. This approach eliminates one parameter from the problem; moreover, the linear stability properties of the conduction state now depend only on the product $Ra(Le - 1)$ [22]. The linear analysis for a vertically infinite system was carried out by Xin et al. [23]. Ghorayeb and Mojtabi [22] present the corresponding results for bounded domains as a function of the aspect ratio A of the cavity. Symmetry considerations of the equations indicate that, depending on A, the primary steady state bifurcation is either a pitchfork or a transcritical bifurcation. For aspect ratio $A = 1$, Xin et al. [23] and Bergeon et al. [24] computed the solution branches emerging from these bifurcations using numerical continuation and showed that near the transcritical bifurcation the solutions take the form of a three roll state. With increasing amplitude supercritical solutions take the form of a large counterclockwise cell slanted across the cavity with smaller cells located in opposite corners, while the subcritical solutions gradually evolve into a single clockwise cell. The pitchfork bifurcation was found to be subcritical. Extensions of this work to inclined cavities have also been discussed [24].

In the next Section we formulate the mathematical problem followed by linear analysis of the pure conductive state as a function of the aspect ratio of the cavity. This analysis locates an important codimension-two bifurcation point A_c at which the conduction state loses stability simultaneously to an odd (antisymmetric) and an even (symmetric) mode. To understand the parameter dependence of the solutions we perform in Section 4 a weakly nonlinear analysis for $A \neq A_c$; this analysis is based on a Galerkin truncation and is performed analytically. Two situations with A near A_c are discussed in detail. The stability of the conduction state with respect to *finite* amplitude perturbations is addressed in Section 5 where an energy method is used to establish the presence of finite amplitude saddle-node bifurcations. Section 6 is devoted to a discussion of the behavior near the codimension-two point and the interaction between the symmetric and antisymmetric states. The results obtained are compared with accurate numerically computed bifurcation diagrams in Section 7. Finally, in Section 8 the analysis is extended to the case $N \neq -1$ with no conduction state present.

2. Mathematical model and basic equations

We consider a two-dimensional container of length L and height H filled with a non-reactive Boussinesq binary fluid mixture (see Fig. 1), and subject to lateral forcing due to imposed temperature and concentration differences:

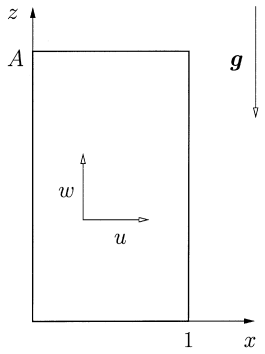

Fig. 1. Cavity configuration.

$T = T_1$, $C = C_1$ at $x = 0$, and $T = T_2$, $C = C_2$ at $x = L$, with $\Delta T \equiv T_1 - T_2 > 0$, $\Delta C \equiv C_1 - C_2 > 0$. The mixture has density ρ, kinematic viscosity ν, and thermal and solutal diffusivities χ and D. Soret and Dufour effects will not be explicitly taken into account but can be easily incorporated in the treatment that follows by means of a transformation that takes the Soret–Dufour equations into those used below (see [25]).

We assume that in the expected range of temperatures and concentrations the density varies linearly with the temperature and concentration,

$$\rho(T, C) = \rho_{\text{ref}}(1 - \beta_T(T - T_{\text{ref}}) - \beta_C(C - C_{\text{ref}})), \tag{1}$$

where ρ_{ref} is the density at temperature $T_{\text{ref}} = T_2$ and concentration $C_{\text{ref}} = C_2$. In the following we assume that the volume expansion coefficients β_T and β_C are constant. For most fluids, β_T is positive. Assuming that C is the concentration of the heavier component, β_C is negative.

The dimensionless temperature and concentration are taken to be $(T - T_{\text{ref}})/(T_1 - T_2)$ and $(C - C_{\text{ref}})/(C_1 - C_2)$. Distance, time and velocity are non-dimensionalized with L, L^2/ν and ν/L, respectively. The resulting dimensionless equations are:

$$\nabla \cdot \boldsymbol{u} = 0, \tag{2}$$

$$\frac{\partial \boldsymbol{u}}{\partial t} + (\boldsymbol{u} \cdot \nabla)\boldsymbol{u} = -\nabla p + \Delta \boldsymbol{u} + Gr(T + NC)\boldsymbol{z}, \tag{3}$$

$$\frac{\partial T}{\partial t} + (\boldsymbol{u} \cdot \nabla)T = \frac{1}{Pr}\Delta T, \tag{4}$$

$$\frac{\partial C}{\partial t} + (\boldsymbol{u} \cdot \nabla)C = \frac{1}{Sc}\Delta C, \tag{5}$$

where $\boldsymbol{u} = u\boldsymbol{x} + w\boldsymbol{z}$ is the dimensionless velocity vector, and $Gr = L^3\beta_T(T_1 - T_2)g/\nu^2$ and $N = \beta_C(C_1 - C_2)/\beta_T(T_1 - T_2)$ are, respectively, the thermal Grashof number and the buoyancy number. The Prandtl, Schmidt and Lewis numbers are given by $Pr = \nu/\chi$, $Sc = \nu/D$ and $Le = Sc/Pr$. For future reference we also define the thermal Rayleigh number $Ra = Pr\,Gr$.

In the dimensionless variables the flow domain is $(x, z) \in \Omega = [0, 1] \times [0, A]$, where $A = H/L$ is the cavity aspect ratio. The horizontal walls are taken to be insulating and across these two walls the normal mass flux is zero. No-slip boundary conditions are imposed along all boundaries. Thus

$$u = w = 0 \quad \text{along } \partial\Omega, \tag{6}$$

$$T(x=1,z)=C(x=1,z)=T(x=0,z)-1=C(x=0,z)-1=0 \quad \forall z\in[0,A], \tag{7}$$

$$\frac{\partial T}{\partial z}(x,z=0,A)=\frac{\partial C}{\partial z}(x,z=0,A)=0 \quad \forall x\in[0,1]. \tag{8}$$

We consider here the particularly interesting situation in which the buoyancy forces due to the thermal and solutal gradients are opposed and equal in magnitude:

$$N=\frac{\beta_C(C_1-C_2)}{\beta_T(T_1-T_2)}=-1. \tag{9}$$

In this case, the double-diffusive state $\boldsymbol{u}=\mathbf{0}$ and $T_0=C_0=1-x$ is a solution of Eqs. (2)–(5) with the boundary conditions (6)–(8).

It is convenient to rewrite Eqs. (2)–(5) as evolution equations for perturbations about this equilibrium state. We denote the perturbation by $(\boldsymbol{u}', p', T', C')$ and introduce the streamfunction ψ' such that $u'=-\partial\psi'/\partial z$ and $w'=\partial\psi'/\partial x$. Eliminating p' we obtain

$$\frac{\partial}{\partial t}\begin{pmatrix}\Delta\psi'\\ T'\\ C'\end{pmatrix}=\begin{pmatrix}\Delta^2 & Gr(\partial/\partial x) & -Gr(\partial/\partial x)\\ -\partial/\partial z & \Delta/Pr & 0\\ -\partial/\partial z & 0 & \Delta/Sc\end{pmatrix}\begin{pmatrix}\psi'\\ T'\\ C'\end{pmatrix}+\begin{pmatrix}N_1(\psi',\psi')\\ N_2(\psi',T')\\ N_2(\psi',C')\end{pmatrix}, \tag{10}$$

where for any pair (f,g) of real functions

$$N_1(f,f)=\frac{\partial f}{\partial z}\left(\frac{\partial^3 f}{\partial x\partial z^2}+\frac{\partial^3 f}{\partial x^3}\right)-\frac{\partial f}{\partial x}\left(\frac{\partial^3 f}{\partial z\partial x^2}+\frac{\partial^3 f}{\partial z^3}\right), \tag{11}$$

$$N_2(f,g)=\frac{\partial f}{\partial z}\frac{\partial g}{\partial x}-\frac{\partial f}{\partial x}\frac{\partial g}{\partial z}. \tag{12}$$

These equations are to be solved subject to the homogeneous boundary conditions:

$$T'(x=1,z)=C'(x=1,z)=T'(x=0,z)=C'(x=0,z)=0 \quad \forall z\in[0,A], \tag{13}$$

$$\frac{\partial T'}{\partial z}(x,z=0,A)=\frac{\partial C'}{\partial z}(x,z=0,A)=0 \quad \forall x\in[0,1] \tag{14}$$

and

$$\left(\frac{\partial\psi'}{\partial x}\right)_{x=0,1}=\left(\frac{\partial\psi'}{\partial z}\right)_{z=0,A}=(\psi')_{\partial\Omega}=0. \tag{15}$$

Eqs. (10) with boundary conditions (13)–(15) are invariant under rotations by π about the point $(1/2, A/2)$. This rotation is described by the operator S defined by

$$S\begin{pmatrix}\psi'\\ T'\\ C'\end{pmatrix}(x,z)=\begin{pmatrix}\psi'\\ -T'\\ -C'\end{pmatrix}(1-x,A-z) \tag{16}$$

and is a generalized reflection since $S^2=1$. The resulting symmetry group $\boldsymbol{Z}_2\equiv\{I,S\}$ plays an important role in the bifurcation analysis described in Section 4. In particular, it is known that in the presence of this symmetry group, the conduction state can only lose stability to states that are either symmetric or antisymmetric with respect to S [26]. The former occurs when the marginally stable eigenfunction is invariant under S; the latter when it breaks invariance under S. The next two sections provide a concrete illustration of these results using the evolution equations (10) with the boundary conditions (13)–(15).

3. Linear stability

In this section we describe the stability properties of the conduction state for aspect ratios $A = 1$ and $A = 2.6$ and parameter values typical of molten salts, i.e., $Pr \sim 1$, $Sc \sim 10 - -100$ [27]. The choice of aspect ratios follows Ghorayeb and Mojtabi [22] and Bergeon et al. [24]. The linearized equations (10) have solutions of the form $(\psi', T', C')(x, z)\exp((\sigma + \mathrm{i}\omega)t)$, where ω is a real number and $\mathrm{i} = \sqrt{-1}$. At a steady bifurcation $\sigma = \omega = 0$, whereas at a Hopf bifurcation $\sigma = 0$ and $\omega \neq 0$. The bifurcation points are located by solving the system

$$\Delta(\Delta - \mathrm{i}\omega)\psi' = Gr\frac{\partial(C' - T')}{\partial x}, \tag{17}$$

$$(\Delta - Pr\,\mathrm{i}\omega)T' = Pr\frac{\partial\psi'}{\partial z}, \tag{18}$$

$$(\Delta - Sc\,\mathrm{i}\omega)C' = Sc\frac{\partial\psi'}{\partial z}. \tag{19}$$

This is done by means of a Galerkin method using the following expansions:

$$\psi'(x, z) = \sum_{i=0}^{n}\sum_{j=0}^{m} a_{ij}\sin(\pi x)\sin(i\pi x)\sin(\pi z/A)\sin(j\pi z/A), \tag{20}$$

$$T'(x, z) = \sum_{i=0}^{n}\sum_{j=0}^{m} b_{ij}\sin(i\pi x)\cos(j\pi z/A), \tag{21}$$

$$C'(x, z) = \sum_{i=0}^{n}\sum_{j=0}^{m} c_{ij}\sin(i\pi x)\cos(j\pi z/A). \tag{22}$$

These expansions satisfy the boundary conditions (13)–(15). Substitution into Eqs. (10) yields a linear algebraic system of the form $\mathcal{L}\boldsymbol{X} = \boldsymbol{0}$ with $\boldsymbol{X} = (a_{ij}, b_{ij}, c_{ij})_{i=0,n;\,j=0,m}$. For particular values (Gr, ω), the determinant of $\mathcal{L}$ is zero indicating a bifurcation point. Fig. 2 shows the modulus of the determinant for $Pr = 1$, $Sc = 11$, when

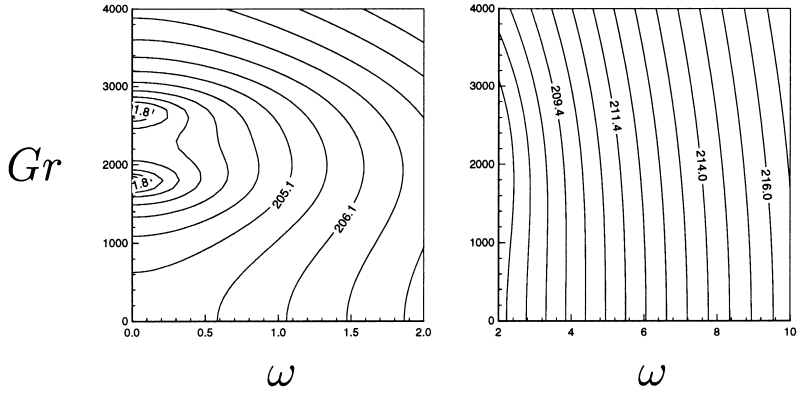

Fig. 2. Isovalues of the modulus of the determinant det $\mathcal{L}$ for $Pr = 1$, $Sc = 11$, $A = 1$ and (5,4) modes truncation.

$A = 1$ and a $m = (5, 4)$ mode truncation is used. For $0 < \omega < 10$ and $0 < Gr < 4000$ the results indicate that no Hopf bifurcation occurs. Fig. 2 indicates that there are two steady state bifurcations ($\omega = 0$) at $Gr = 1795$ and $Gr = 2728$. With seven modes one finds that these bifurcations occur at $Gr = 1717$ and $Gr = 2590$, respectively. The corresponding results for $A = 2.6$ are $Gr = 934$ and $Gr = 942$ for the (5,4) mode truncation and $Gr = 765$ and $Gr = 805$ for the fully resolved calculation. For $A = 1$ and $A = 2.6$ no Hopf bifurcations were found for the following parameter combinations $(Pr, Sc) = (1, 2), (1, 5), (1, 20), (10, 15)$ and $(10, 50)$.

Within the Galerkin truncation the steady state bifurcations can be studied analytically. Due to the $\boldsymbol{Z}_2$ symmetry, the associated eigenmodes are either symmetric with respect to S, i.e., $S(\psi', T', C') = (\psi', T', C')$, or antisymmetric, i.e., $S(\psi', T', C') = -(\psi', T', C')$. The symmetric eigenmodes contain an odd number of cells, whereas the antisymmetric ones contain an even number of cells. Eqs. (20)–(22) indicate that the contribution to the symmetric modes comes from terms with $i + j$ even, while the contribution to the antisymmetric modes comes from terms with $i + j$ odd. The linear stability problem thus splits into two separate problems:

$$\mathcal{L}\boldsymbol{X} = \begin{pmatrix} (M_{Gr}) & 0 \\ 0 & (N_{Gr}) \end{pmatrix} \begin{pmatrix} \begin{pmatrix} a_{ij} \\ b_{ij} \\ c_{ij} \end{pmatrix}_{i+j \text{ even}} \\ \begin{pmatrix} a_{ij} \\ b_{ij} \\ c_{ij} \end{pmatrix}_{i+j \text{ odd}} \end{pmatrix} = \begin{pmatrix} 0 \\ 0 \end{pmatrix}, \tag{23}$$

where (M_{Gr}) and (N_{Gr}) are matrices. We used the software MAPLE to find the values of Gr, a_{ij}, b_{ij} and c_{ij} at which $\det \mathcal{L} = \omega = 0$; $\det(M_{Gr}) = 0$ at a bifurcation to a symmetric mode, while $\det(N_{Gr}) = 0$ at a bifurcation to an antisymmetric one. The analytical calculations reported below were all carried out with $n = m = 4$ for ψ' and $n = m = 3$ for T' and C'.

Elimination of the variables C', T' from Eqs. (17)–(19) in favor of ψ' shows that the solution of the linear stability problem determines the product $Gr_c|Sc - Pr|$. It follows that the lowest value of the thermal Grashof number for symmetric eigenmodes is given by an expression of the form

$$Gr_c = \left| \frac{1}{Sc - Pr} \right| f(A), \tag{24}$$

with a similar expression for the lowest value of the thermal Grashof number for antisymmetric eigenmodes:

$$Gr_c = \left| \frac{1}{Sc - Pr} \right| g(A). \tag{25}$$

Here f and g are two real functions of the aspect ratio. The graphs of f and g from the (4, 3) truncation are shown in Fig. 3; seven modes in each field are required to reproduce accurately the results obtained by Bergeon et al. [24] and Xin et al. [23] for $1 < A < 3.4$.

Fig. 3 shows that the neutral stability curves $Gr_c(A)$ for the two modes cross at $A_c \approx 2.526$; for $A < A_c$ the first instability is to a symmetric mode, while for $A > A_c$ it is antisymmetric close to the onset. The point $A = A_c$ is called a mode interaction point: at this point the conduction state loses stability simultaneously to modes of both types. As discussed by Riley and Winters [28], Winters et al. [29] and Hirschberg and Knobloch [30] mode interaction between odd and even modes is typical in systems with reflection symmetry. For example, in two-dimensional Boussinesq convection with no-slip sidewall boundary conditions the marginal stability curves for symmetric and antisymmetric modes cross repeatedly with increasing aspect ratio.

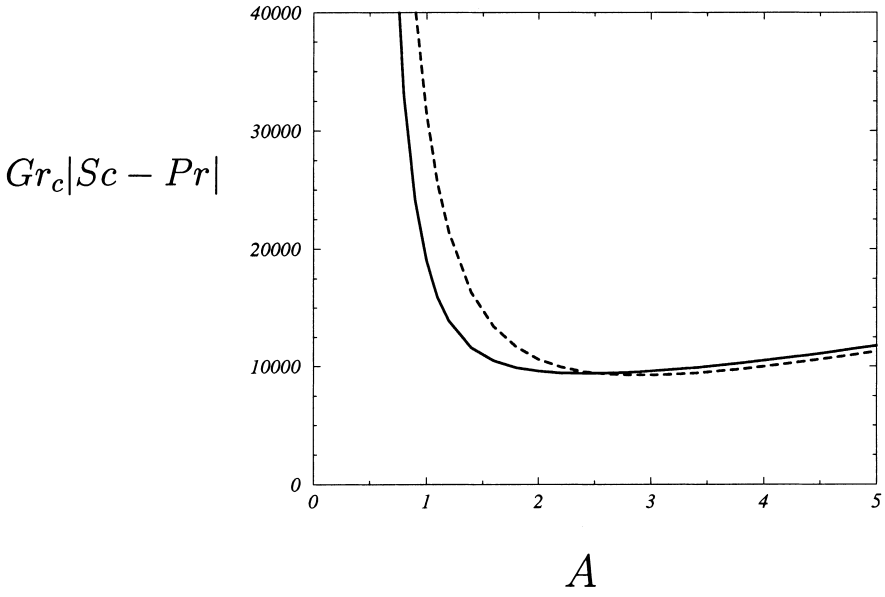

Fig. 3. Critical Grashof numbers of the first two steady primary bifurcations using four modes for the streamfunction and the temperature and concentration fields. Continuous (dashed) line indicates bifurcation to a symmetric (antisymmetric) mode. The computations were carried out with $n = m = 4$ for ψ' and $n = m = 3$ for T' and C'.

In the next section we use the Galerkin truncation to analyze the parameter dependence of the codimension-one bifurcations arising when Gr is increased for $A = 1$ and $A = 2.6$ and perform analytically the required center-manifold reduction [31] to describe the resulting weakly nonlinear state and its stability. The codimension-two mode interaction point is considered in Section 6.

4. Weakly nonlinear analysis

In the weakly nonlinear regime the properties of the system are captured by simpler equations called normal forms. Appendix A summarizes the details of the derivation of these equations from Eqs. (10) for the two cases of interest, when the primary bifurcation is to a symmetric state and to an antisymmetric state. Both reductions are valid near the onset of the primary instability, i.e., for $|Gr - Gr_c|/Gr_c \ll 1$, where Gr_c denotes the corresponding critical Grashof number. In either case the reduction procedure yields an equation of the form

$$\frac{\mathrm{d}K}{\mathrm{d}\tau} = V(Gr - Gr_c, K), \tag{26}$$

where K measures the amplitude of the unstable mode and τ is a suitable slow time. In the following we define the quantity s by $S(K\phi) = s(K)\phi$, where $\phi(x, z)$ is an eigenmode of $\mathcal{L}$. Since $V(Gr - Gr_c, K)$ is derived by a procedure that preserves the symmetries of the original problem $V(Gr - Gr_c, K)$ must also respect these symmetries, i.e., $s(V(Gr - Gr_c, K)) = V(Gr - Gr_c, s(K))$. This is the requirement of equivariance [26,32]. We refer to $s = 1$ as the symmetric case, and to $s = -1$ as the antisymmetric case.

In the symmetric case we obtain the normal form

$$\frac{\partial K_s}{\partial t^{(1)}} = V(Gr - Gr_c, K_s) \equiv \frac{K(Gr^{(1)}|Pr - Sc| + K_s(b + (Pr + Sc)c))}{(d + (Pr + Sc)e)} \tag{27}$$

with

$$b = \langle N_1(f_1, f_1), f_1^* \rangle \Big/ \left\langle \frac{\partial f_2}{\partial x}, f_1^* \right\rangle, \tag{28}$$

$$c = \langle N_2(f_1, f_2), f_2^* \rangle \Big/ \left\langle \frac{\partial f_2}{\partial x}, f_1^* \right\rangle, \tag{29}$$

$$d = \langle \Delta f_1, f_1^* \rangle \Big/ \left\langle \frac{\partial f_2}{\partial x}, f_1^* \right\rangle, \tag{30}$$

$$e = \langle f_2, f_2^* \rangle \Big/ \left\langle \frac{\partial f_2}{\partial x}, f_1^* \right\rangle. \tag{31}$$

In these expressions the quantity $\langle X, Y \rangle$ represents the scalar product $\int\int_\Omega XY \, \mathrm{d}x \, \mathrm{d}z$; $Gr^{(1)} \equiv (Gr - Gr_\mathrm{c})/\varepsilon$ is the bifurcation parameter and εK_s is the amplitude of the symmetric mode evolving on the timescale $t^{(1)} \equiv t/\varepsilon$.

In the antisymmetric case the quadratic term must vanish and the reduction must be carried to third order. The result is (see Appendix A)

$$\frac{\partial K_\mathrm{a}}{\partial t^{(2)}} \equiv V(Gr - Gr_\mathrm{c}, K) = \frac{K_\mathrm{a}(Gr^{(2)}|Sc - Pr| + K_\mathrm{a}^2(b + (Pr^2 + Sc^2)c + f(Pr + Sc) + g\, Pr\, Sc))}{(d + (Pr + Sc)e)}, \tag{32}$$

where $Gr^{(2)} \equiv (Gr - Gr_\mathrm{c})/\varepsilon^2$ is now the bifurcation parameter and εK_a is the amplitude of the antisymmetric mode evolving on the slower timescale $t^{(1)} \equiv t/\varepsilon^2$. We omit the detailed expressions for the coefficients.

4.1. Case $A = 1$: the symmetric case $S(f_1(x, z)) = f_1(x, z)$

For aspect ratio $A = 1$ the critical eigenmode is invariant under the symmetry S. For the streamfunction this property implies that

$$S(\psi'(x, z, t^{(1)})) \equiv \psi'(1 - x, A - z, t^{(1)}) = \psi'(x, z, t^{(1)}) \tag{33}$$

and consequently that

$$s(K) = K, \tag{34}$$

where K is the amplitude of the symmetric mode. Thus the symmetry S does not impose any constraint on the amplitude equation (27), i.e., we expect $V(Gr - Gr_\mathrm{c}, K)$ to satisfy the non-degeneracy conditions:

$$\frac{\partial^2 V}{\partial (Gr - Gr_\mathrm{c}) \partial K}(0, 0) \neq 0 \quad \text{and} \quad \frac{\partial^2 V}{\partial^2 K}(0, 0) \neq 0. \tag{35}$$

These properties indicate that the bifurcation is transcritical. Thus near the bifurcation point the amplitude of the streamfunction is a linear function of the thermal Grashof number.

Our symbolic computations confirm these expectations and give $b \approx -1120$, $c \approx 1302124$, $d \approx 292$ and $e \approx 890$; the purely diffusive solution $K = 0$ is stable if and only if $Gr^{(1)} < 0$, i.e., for thermal Grashof numbers smaller than the critical thermal Grashof number. From relation (27), we now obtain the equation of the bifurcating branch:

$$\psi \approx \varepsilon \psi^{(1)} = -\frac{1}{b + (Pr + Sc)c}(Gr - Gr^{(0)})|Sc - Pr| f_1(x, z). \tag{36}$$

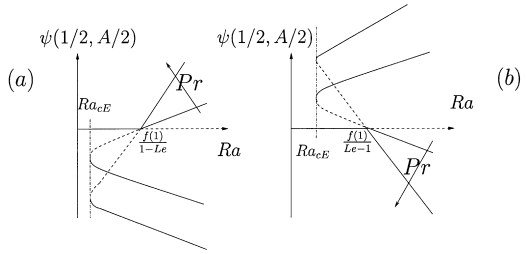

Fig. 4. Schematic bifurcation diagram, at fixed Le, showing the streamfunction at the center of the cavity as a function of the Rayleigh number Ra for (a) $Le < 1$ and (b) $Le > 1$. Positive ψ indicates clockwise rotation. The slope at the primary bifurcation increases as Pr decreases.

For the computed values of b, c, d and e, Eq. (27) shows that the convective solution $K \neq 0$ is linearly stable for $Gr^{(1)} > 0$, while $K \neq 0$ is linearly unstable for $Gr^{(1)} < 0$.

This analytical approach allows us to understand the sense of rotation of the flow. We found that f_1 is positive (resp. negative) at $x = z = 0.5$ for $Le > 1$ (resp. $Le < 1$). For most fluids, $b + (Pr + Sc)c$ is positive and consequently, for $Gr^{(1)} > 0$, the streamfunction at the midpoint is negative when $Le > 1$ and positive when $Le < 1$. This implies that the sense of rotation is counterclockwise for $Le > 1$ and clockwise for $Le < 1$. This result is sensible: when $Le > 1$ the sense of rotation is determined by the concentration of the heavier component since temperature perturbations diffuse away more rapidly. A counterclockwise flow produces a negative concentration perturbation in the upper half of the cell and a positive perturbation in the lower half. The resulting concentration distribution opposes the flow and results in equilibration at small amplitude. In contrast, a clockwise flow produces a positive concentration perturbation in the upper half which tends to accelerate the flow. Thus when $Le > 1$ we associate a counterclockwise flow with the small amplitude supercritical state, and a clockwise flow with the unstable subcritical branch. This interpretation is confirmed in Section 8. When $Le < 1$ the sense of rotation is determined instead by the temperature and the circulations are reversed.

Fig. 4 shows the dependence of the streamfunction amplitude on Ra in the two cases $Le > 1$ and $Le < 1$. Solid lines correspond to stable solution branches and dashed lines to linearly unstable solutions. The two situations ($Le < 1$ or $Le > 1$) are identical except for the opposite sense of rotation. In the following we therefore only consider the case $Le > 1$. Fig. 5 shows the flow structure of the critical eigenmode for $Le = 11$ and $Pr = 1$ confirming that the eigenmode is symmetric. The critical Rayleigh number depends only Le and is equal to $f(1)/|Le - 1|$, but the slope of the non-trivial solution branches emerging at the transcritical bifurcation depends on both the Prandtl and Schmidt numbers. In particular, relation (36) shows that at fixed Le the slope increases when the Prandtl number decreases. We return to this point in Sections 5 and 6.

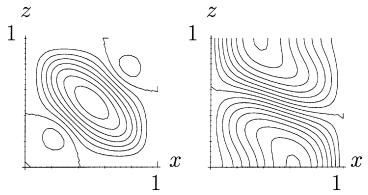

Fig. 5. Streamlines (left) and isovalues of temperature perturbations (right) of the critical eigenmode for $A = 1$, $Le = 11$ and $Pr = 1$.

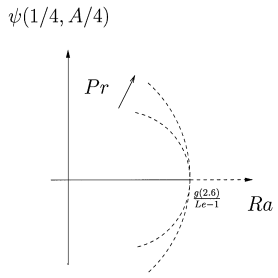

Fig. 6. Schematic bifurcation diagram, at fixed Le, showing the streamfunction ψ at $x = z = 0.25$ as a function of the Rayleigh number Ra. The slope increases (in magnitude) as Pr decreases.

4.2. Case $A = 2.6$: the antisymmetric case $S(f_1(x, z)) = -f_1(x, z)$

In this case the critical eigenmode is antisymmetric,

$$S(\psi'(x, z, t^{(1)})) \equiv \psi'(1 - x, A - z, t^{(1)}) = -\psi'(x, z, t^{(1)}), \tag{37}$$

and hence

$$s(K) = -K. \tag{38}$$

Consequently, equivariance requires that

$$V(Gr - Gr_c, -K) = -V(Gr - Gr_c, K), \tag{39}$$

implying that the condition $(\partial^2 V/\partial^2 K)(0, 0) \neq 0$ fails. One now expects a non-degenerate pitchfork bifurcation provided that $(\partial^3 V/\partial^3 K)(0, 0) \neq 0$. Our symbolic calculations confirm that all quadratic terms vanish and yield the values $b \approx 3280,\ c \approx 10\,553\,802,\ d \approx 320,\ e \approx 1193,\ f \approx 1\,298\,192$ and $g \approx 21\,207\,874$ for the coefficients in the normal form (32). Thus for any value of Pr and Sc, the pitchfork bifurcation is subcritical and the emerging solutions are linearly unstable. The convection amplitude is given by

$$\psi^2 \approx \varepsilon^2 \psi^{(1)2} = -\frac{f_1^2}{b + (Pr^2 + Sc^2)c + f(Pr + Sc) + g\ Pr\ Sc}(Gr - Gr^{(0)})|Sc - Pr|. \tag{40}$$

Fig. 6 shows a schematic representation of the resulting bifurcation diagram. For a fixed Lewis number the curvature of the solution branches near onset decreases when the Prandtl number decreases (see (32)). Fig. 7 shows the structure of this critical eigenmode when $Le = 11$ and $Pr = 1$ confirming that the flow structure and isotherm perturbations are antisymmetric.

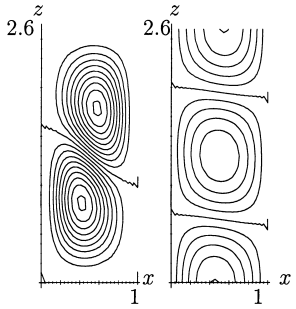

Fig. 7. Streamlines (left) and isotherm perturbations (right) of the critical eigenmode for $A = 2.6$, $Le = 11$ and $Pr = 1$.

4.3. Heat and mass transfer

We now turn to the characterization of the transport efficiency of the resulting motion. Using the asymptotic expansion in the vicinity of the bifurcation point we obtain the following expressions for the Nusselt and the Sherwood numbers $Nu(x)$ and $Sh(x)$:

$$Nu(x) \equiv -\int \frac{\partial T}{\partial x}\mathrm{d}z = 1 - \varepsilon\, Pr\, K \int \frac{\partial f_2}{\partial x}\mathrm{d}z - \varepsilon^2 \int \frac{\partial T^{(2)}}{\partial x}\mathrm{d}z - \cdots, \tag{41}$$

$$Sh(x) \equiv -\int \frac{\partial C}{\partial x}\mathrm{d}z = 1 - \varepsilon\, Sc\, K \int \frac{\partial f_2}{\partial x}\mathrm{d}z - \varepsilon^2 \int \frac{\partial C^{(2)}}{\partial x}\mathrm{d}z - \cdots. \tag{42}$$

These quantities measure, respectively, the dimensionless horizontal heat and concentration fluxes. In these expressions the order ε terms vanish. At order ε^2 one finds that

$$(Sh - 1) = Le^2(Nu - 1). \tag{43}$$

This relation describes the relative efficiency with which heat and concentration are transported in the weakly nonlinear regime; we find, however, that in the strongly nonlinear regime this relation between the fluxes no longer holds.

Result (43) follows from the second order relation (see Appendix A)

$$-\frac{1}{Pr}\frac{\partial \psi^{(2)}}{\partial z} + \frac{1}{Sc}\frac{\partial \psi^{(2)}}{\partial z} + \frac{\Delta T^{(2)}}{Pr^2} - \frac{\Delta C^{(2)}}{Sc^2} = 0. \tag{44}$$

Integration of (44) from $z = 0$ to $z = 1$ together with expressions (20)–(22) now yields

$$c_{i0} = Le^2 b_{i0} \tag{45}$$

for all i and hence the relation (43).

5. The energy method

In this Section, we compute the critical Grashof number above which finite amplitude perturbations grow. In order to do this we rescale the variables T and C: $T \to T/\sqrt{\lambda\, Gr}$, $C \to C/\sqrt{\mu\, Gr}$ and let $R = \sqrt{Gr}$. Eqs. (2)–(5) become:

$$\nabla \cdot \boldsymbol{u} = 0, \tag{46}$$

$$\frac{\partial \boldsymbol{u}}{\partial t} + (\boldsymbol{u}\cdot\nabla)\boldsymbol{u} = -\nabla p + \Delta \boldsymbol{u} + R\left(\frac{T}{\sqrt{\lambda}} - \frac{C}{\sqrt{\mu}}\right)\boldsymbol{z}, \tag{47}$$

$$\frac{\partial T}{\partial t} + (\boldsymbol{u}\cdot\nabla)T = -R\sqrt{\lambda}\boldsymbol{u}\cdot\nabla(1-x) + \frac{1}{Pr}\Delta T, \tag{48}$$

$$\frac{\partial C}{\partial t} + (\boldsymbol{u}\cdot\nabla)C = -R\sqrt{\mu}\boldsymbol{u}\cdot\nabla(1-x) + \frac{1}{Sc}\Delta C, \tag{49}$$

with the boundary conditions (6)–(8). Here λ and μ are positive real numbers. Next we define a positive functional which is a measure of the energy E of the perturbations:

$$E = \frac{1}{2}\int\int_{\Omega} (\boldsymbol{u}\cdot\boldsymbol{u} + T^2 + C^2)\,\mathrm{d}\Omega. \tag{50}$$

The temporal evolution of this energy is given by

$$\frac{\mathrm{d}E}{\mathrm{d}t} = -A_1^2\left(1 - R\frac{A_2}{A_1^2}\right), \tag{51}$$

where

$$A_1^2 = \int\int_{\Omega}\left(|\nabla \boldsymbol{u}|^2 + \frac{|\nabla T|^2}{Pr} + \frac{|\nabla C|^2}{Sc}\right)\mathrm{d}\Omega, \tag{52}$$

$$A_2 = \int\int_{\Omega}\left(\left(\frac{T}{\sqrt{\lambda}} - \frac{C}{\sqrt{\mu}}\right)\boldsymbol{u}\cdot\boldsymbol{z} - \sqrt{\lambda}T\boldsymbol{u}\cdot\nabla(1-x) - \sqrt{\mu}C\boldsymbol{u}.\nabla(1-x)\right)\mathrm{d}\Omega. \tag{53}$$

It follows that there is a positive (modified) Grashof number R_c below which the pure conduction state is the only solution of the problem. This critical number is defined by the condition $(1/R_c) = \max(A_2)$ subject to the constraints $A_1^2 = 1$ and $\nabla\cdot\boldsymbol{u} = 0$ in Ω. Thus for $R < R_c$ the energy E of the perturbation necessarily decays to zero as $t \to \infty$ [33]; R_c also provides the lower limit on the Grashof number at which a saddle-node bifurcation can be present and hence on the extent of any hysteresis between the conduction and finite amplitude states.

The associated Euler–Lagrange equations written in the perturbation variables ψ', T' and C' are

$$2\Delta T' - R\,Pr\left(\sqrt{\lambda}\frac{\partial\psi'}{\partial z} - \frac{1}{\sqrt{\lambda}}\frac{\partial\psi'}{\partial x}\right) = 0, \tag{54}$$

$$2\Delta C' - R\,Sc\left(\sqrt{\mu}\frac{\partial\psi'}{\partial z} - \frac{1}{\sqrt{\mu}}\frac{\partial\psi'}{\partial x}\right) = 0, \tag{55}$$

$$2\Delta^2\psi' - R\left(\sqrt{\lambda}\frac{\partial T'}{\partial z} - \frac{1}{\sqrt{\lambda}}\frac{\partial T'}{\partial x} + \sqrt{\mu}\frac{\partial C'}{\partial z} - \frac{1}{\sqrt{\mu}}\frac{\partial C'}{\partial x}\right) = 0. \tag{56}$$

with the boundary conditions (13)–(15).

To solve these equations the perturbations are expanded as in the preceding linear stability analysis. The solution determines the eigenvalue R as a function of λ and μ. We now seek the maximum of this value over all possible values of λ and μ in order to identify the largest range of values of R in which the energy necessarily decays. For any (m, n) truncation the corresponding value of R provides a *lower* bound on the critical Rayleigh number Ra_{cE} below which convection ceases. Since Eqs. (54)–(56), written as a single equation, depend only on the Rayleigh and Lewis numbers the value of Ra_{cE} depends only on the aspect ratio and Le. Fig. 8 shows the Lewis number dependence of the critical Rayleigh number Ra_c for the onset of linear instability of the conduction state, and of the critical Rayleigh number Ra_{cE} obtained by the energy method, when $A = 1$ and $A = 2.6$, computed using $n = m = 22$ for $A = 1$ and $n = 20$, $m = 28$ for $A = 2.6$. These truncations ensure the convergence of the Galerkin method. When $Le \to \infty$, the product $Ra_{cE}\,Le \to 6940$ for $A = 1$ and 4530 for $A = 2.6$. It follows that the saddle-node bifurcation at which the subcritical solution branch turns around must lie between the two curves shown in Fig. 8. We show the streamfunctions for these two aspect ratios obtained from Eqs. (54)–(56) at Ra_{cE} in Fig. 9. As expected both are *symmetric* and consist of a clockwise (resp. counterclockwise) one-cell flow for $Le > 1$ (resp. $Le < 1$). These results are in agreement with the extrapolation of the weakly nonlinear ones obtained for the subcritical transcritical branch in Section 4.1 (see Fig. 4), although it must be emphasized that when $A > A_c$ there may be regimes in which the lowest-lying saddle-node lies on the branch of *antisymmetric* solutions; in this case the variational solution would have a structure quite different from that shown in Fig. 9. Note that at fixed Lewis number Ra_{cE} is uniquely determined (and independent of the Prandtl number), while the amplitude of the variational solution increases as Pr decreases.

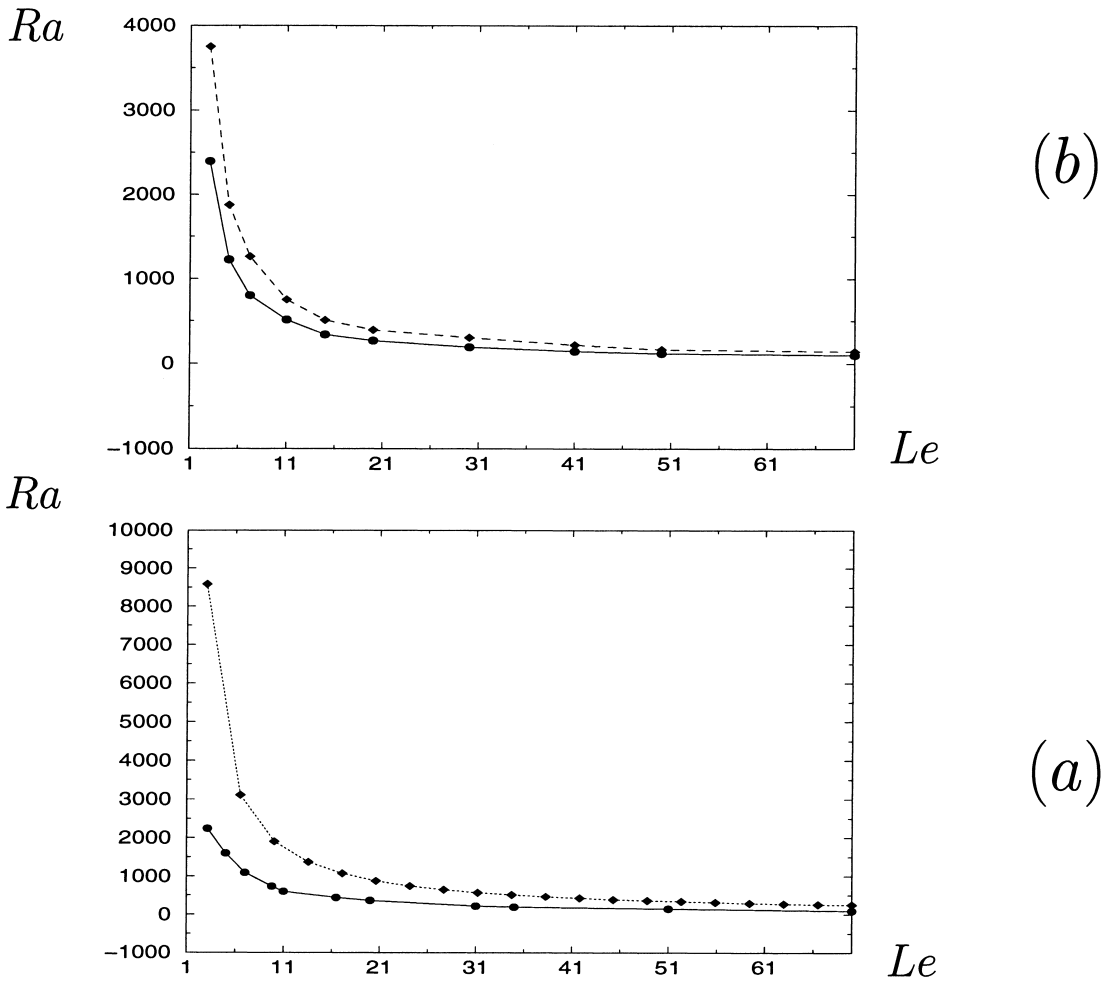

Fig. 8. (a) Linear theory critical Rayleigh number Ra_c (filled diamonds) and energy critical Rayleigh number Ra_{cE} (filled circles) versus the Lewis number Le when $A = 1$. The computations were carried out with $n = m = 22$ for ψ', T' and C'. (b) Linear theory critical Rayleigh number Ra_c (filled diamonds) and energy critical Rayleigh number Ra_{cE} (filled circles) versus the Lewis number Le when $A = 2.6$. The computations were carried out with $n = 20$ and $m = 28$ for ψ', T' and C'.

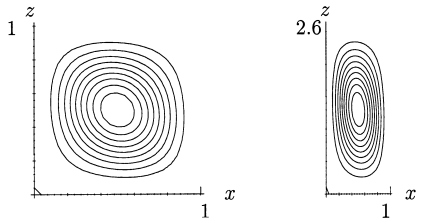

Fig. 9. Streamlines of the variational solution at Ra_{cE} when $A = 1$ (left) and $A = 2.6$ (right) and $Le = 11$, $Pr = 1$. In both cases the flow is clockwise.

6. Mode interaction

In this section we analyze the mode interaction that takes place at $A = A_c$. At this aspect ratio the conduction state loses stability simultaneously to an antisymmetric mode and a symmetric mode. Near $A = A_c$ these two modes are set in close succession and therefore interact at small amplitude. To study this interaction we denote the amplitudes of these modes by K_a and K_s, respectively, and consider finite values of Pr for which the bifurcation to the symmetric mode at A_c is transcritical. The resulting interaction between transcritical and pitchfork bifurcations has been analyzed by Langford [34] in the context of his study of Hopf-steady-state mode interactions. Wittenberg and Holmes [35] provide an extensive review of this type of analysis and its usefulness to PDE investigations, again in the context of Hopf-steady-state interaction. We summarize here the relevant results.

Since the equations for (K_a, K_s) must commute with $s : (K_a, K_s) \to (-K_a, K_s)$ they take the form (to third order in the amplitudes)

$$\tau_0 \frac{dK_a}{dt} = \mu_a K_a + \tau_1 K_s K_a + \tau_2 K_a^3 + \tau_3 K_s^2 K_a + \mathcal{O}(4), \tag{57}$$

$$\sigma_0 \frac{dK_s}{dt} = \mu_s K_s + \sigma_1 K_a^2 + \sigma_2 K_s^2 + \sigma_3 K_a^2 K_s + \sigma_4 K_s^3 + \mathcal{O}(4), \tag{58}$$

where μ_s and μ_a are linear combinations of $Gr - Gr_c$, $A - A_c$. Here Gr_c and A_c are the critical Grashof number and aspect ratio at which the two primary bifurcations coalesce. The quantities σ_i $(i = 0, \ldots, 4)$ and τ_i $(i = 0, \ldots, 3)$ are real functions of the Prandtl and Schmidt numbers; provided appropriate degeneracy conditions are satisfied these can be calculated at $Gr = Gr_c$, $A = A_c$.

Much of the resulting behavior (but not all) is captured by the truncation of these equations at *second order*. A simple rescaling then yields the system

$$\dot{r} = \epsilon r + arz + \mathcal{O}(3), \quad \dot{z} = \delta z + br^2 - z^2 + \mathcal{O}(3), \tag{59}$$

where $a = -\sigma_0\tau_1/\tau_0\sigma_2$, $b = -\operatorname{sgn}\sigma_1\sigma_2$, and $\epsilon = \mu_a/\tau_0$, $\delta = \mu_s/\sigma_0$. Thus $b = \pm 1$. In all cases the fixed point at the origin becomes unstable via a transcritical bifurcation at $\delta = 0$ giving rise to a non-trivial equilibrium $(r_0, z_0) = (0, \delta)$. This fixed point (hereafter PM), corresponding to the *symmetric* states, may then undergo a further pitchfork bifurcation, at $\delta = -\epsilon/a$, generating the steady states $(r_0, z_0) = (\pm\sqrt{(b\epsilon/a)((\epsilon/a) + \delta)}, -\epsilon/a)$. These states are in turn born in a pitchfork bifurcation at $\epsilon = 0$ and correspond to the *antisymmetric* states. This is because near $\epsilon = 0$, $|z_0| \ll |r_0| \ll 1$; however, with increasing amplitude these states gradually cease to be antisymmetric and become *mixed parity* states; we call them mixed modes (hereafter MM). In most cases nothing else happens locally near $(\epsilon, \delta) = (0, 0)$. However, in the case $a > 0$, $b = -1$ the state (r_0, z_0) undergoes a Hopf bifurcation as ϵ increases through $-a\delta/2$, $\delta > 0$ [34]. As also noted in [34], this bifurcation is degenerate within the quadratic truncation. Thus to determine the direction of branching it is necessary to include cubic terms as in Eqs. (57) and (58). Our calculations, summarized in Fig. 10, suggest that this situation does not in fact arise in the present problem. Instead, the results are consistent with Eqs. (59) provided $a < 0$, $b < 0$ with $\delta > 0$ when $\epsilon = 0$.

As already mentioned numerical calculations reveal that the transcritical state $(0, z)$ acquires stability at a secondary saddle-node bifurcation (see Fig. 11). Such a bifurcation can be included in the above analysis by rewriting Eqs. (59) in the form

$$\dot{r} = \epsilon r + arz + cr^3 + drz^2 + \mathcal{O}(4), \quad \dot{z} = \delta z + br^2 - \eta z^2 + er^2 z + fz^3 + \mathcal{O}(4), \tag{60}$$

where η is a third unfolding parameter and $f < 0$. When $\eta \ll 1$ the secondary saddle-node bifurcation occurs at small amplitude and is correctly captured by Eqs. (60). Numerically we find that η is small for small values of Pr.

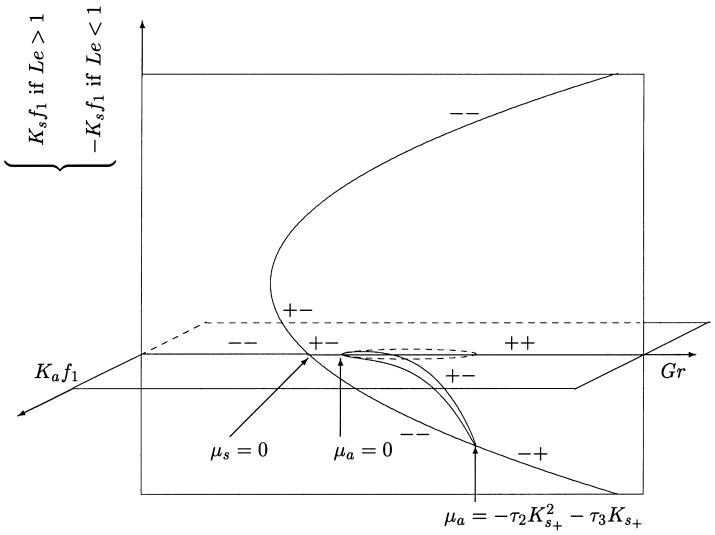

Fig. 10. Schematic 3D bifurcation diagram showing the product $K_s f_1$ (if $Le > 1$) or $-K_s f_1$ (if $Le < 1$) at the center of the cavity as a function of the thermal Grashof number Gr when $A < A_c$. The symmetric solutions lie in the vertical plane and the antisymmetric ones in the horizontal plane. The signs of the stability eigenvalues obtained from the system (57) and (58) are indicated along each branch, with the first describing stability relative to symmetric perturbations and the second relative to antisymmetric perturbations.

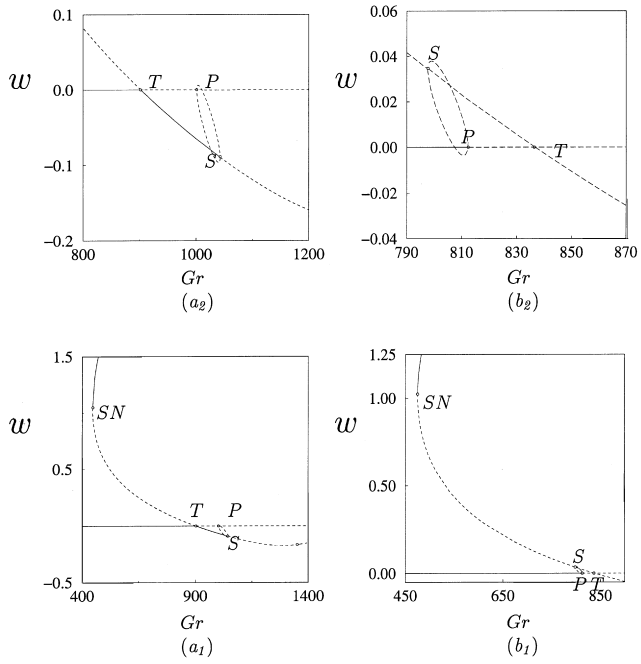

Fig. 11. (a_1) The vertical velocity $w(x = 0.388, 0.5)$ in a container of aspect ratio $A = 1.8$ as a function of Gr. The resolution is 15×19. (a_2) Enlargement of (a_1). (b_1) The corresponding bifurcation diagram for aspect ratio $A = 2.3$ with resolution 15×25. (b_2) Enlargement of (b_1). Stable (unstable) solutions are indicated by continuous (dashed) lines.

The steady states are now given by

$$\text{PM}\ \ (0, z_0): \quad \delta - \eta z_0 + f z_0^2 = 0 \tag{61}$$

and

$$\text{MM}\ \ (r_0, z_0): \quad \epsilon + a z_0 + c r_0^2 + d z_0^2 = 0, \quad \delta z_0 + b r_0^2 - \eta z_0^2 + e r_0^2 z_0 + f z_0^3 = 0. \tag{62}$$

The stability of the pure mode $(0, z_0)$ is determined by the eigenvalues

$$s_1 = \delta - 2\eta z_0 + 3 f z_0^2, \qquad s_2 = \epsilon + a z_0 + d z_0^2. \tag{63}$$

The saddle-node bifurcation occurs when $s_1 = 0$, i.e., at $z_0 = \eta/2f$, $\delta = \eta^2/4f$, cf. Fig. 10. The pitchfork to MM occurs when $s_2 = 0$.

An interesting possibility arises when s_2 vanishes at the saddle-node. This occurs at the codimension-two point

$$\epsilon_c = -\frac{a\eta}{2f} - \frac{d\eta^2}{4f^2}, \qquad \delta_c = \frac{\eta^2}{4f}. \tag{64}$$

At this point there is a codimension-two bifurcation on the PM branch. This bifurcation is an interaction between a saddle-node and a pitchfork bifurcation and is described by the normal form [31,34]:

$$\dot{r} = \mu_1 r + A r z + \mathcal{O}(3), \quad \dot{z} = \mu_2 + B r^2 - z^2 + \mathcal{O}(3), \tag{65}$$

where $z \propto z - z_0$, A and B are coefficients, and μ_1 and μ_2 are new unfolding parameters linearly related to $\epsilon - \epsilon_c$ and $\delta - \delta_c$. As before $|B| = 1$ if r is suitably rescaled. A straightforward calculation shows that

$$A = -\frac{2}{\eta}(a + \mathcal{O}(\eta)), \quad B = -b, \tag{66}$$

$$\mu_1 = \epsilon - \epsilon_c - \frac{a}{\eta}(\delta - \delta_c), \quad \mu_2 = -\frac{\eta^2}{4f}(\delta - \delta_c) + \mathcal{O}(\delta - \delta_c)^2, \tag{67}$$

where $|\epsilon - \epsilon_c| \ll \eta$, $|\delta - \delta_c| \ll \eta^2$. Since Fig. 10 is consistent with the choice $a < 0$, $b < 0$, $\eta > 0$, $f < 0$, it follows that $A > 0$, $B = 1$. This is Case I in the classification of [31]; in this case there is no tertiary Hopf bifurcation on the mixed mode branch, i.e., this codimension-two bifurcation does not introduce any new dynamics. Indeed, a stability calculation for the mixed mode state shows that when $a < 0$, $b = -1$ it is everywhere a saddle, provided that $|\epsilon| \ll 1$, $|\delta| \ll 1$, $|z_0| \ll 1$. These conditions also exclude the presence of a saddle-node bifurcation on the MM branch.

7. Numerical study

7.1. Numerical methods

We used two numerical methods to solve Eqs. (2)–(5): time integration and a continuation method. Time integration was carried out using a pseudo-spectral method. The fields are discretized using the spectral element method [36] with Chebyshev polynomials along the Lobatto–Chebyshev points. The linear terms are integrated implicitly and the nonlinear terms explicitly using the pressure boundary conditions given by Karniadakis et al. [37]. The resulting Poisson problem for the pressure and the Helmholtz problems arising from the diffusion terms are solved using a variational formulation.

The continuation method uses a time integration scheme adapted to compute steady states using a Newton method [38–41]. The linear Newton system is solved using an iterative conjugate gradient method. Once a solution has been computed classical continuation is performed, enabling us to follow any branch of steady solutions.

7.2. Numerical results

We now describe the results of a numerical study of the nonlinear problem using continuation. Since the fully resolved Galerkin truncation shows that $2.11 < A_c < 2.14$ we focus on the two aspect ratios, $A = 1.8$ and $A = 2.3$, fixing $Pr = 1$ and $Sc = 11$. These aspect ratios correspond to the two cases discussed in Section 4. The results are fully resolved and confirm the qualitative conclusions reached on the basis of the analytic but weakly nonlinear calculations using the Galerkin truncation. These conclusions include not only the direction of branching of the two primary branches but also their dependence on the Prandtl and Schmidt numbers.

The results are presented in terms of bifurcation diagrams describing the evolution of a component of the velocity at a given point of the cavity as a function of the thermal Grashof number Gr. The choice of the point is unimportant provided that the variations of the reported quantity clearly exhibit the behavior of the whole solution. In the following, branches of stable (unstable) steady solutions are denoted by continuous (dashed) curves. Although the unstable solutions cannot be observed physically, they indicate how stable solutions are created, annihilated, or related to one another. The subscripts P, T, S and SN denote primary pitchfork, primary transcritical, secondary pitchfork and saddle-node bifurcations, respectively.

When $A = 1.8$ the conduction solution remains stable until $Gr = Gr_T \approx 901.5$ (Fig. 11(a)). At Gr_T it undergoes a transcritical bifurcation, and two branches of convective solutions emerge: a stable supercritical branch present for $Gr > Gr_T$ and an unstable subcritical branch present for $Gr < Gr_T$. Close to Gr_T, the solutions are symmetric three-roll flows. At $Gr_{SN} \approx 445$, the subcritical branch undergoes a saddle-node bifurcation and becomes stable. It remains stable at least up to $Gr = 1300$, the end of our computational domain. Along this stable branch, the solutions consist of symmetric one-roll flow structures. The transition from the three-roll structure to the one-roll structure takes place near the saddle-node: the central roll grows at the expense of the two corner rolls until the corner rolls disappear. During this transition the solution retains its symmetry. The supercritical branch is stable up to Gr_S, $1042.5 < Gr_S < 1042.8$. At Gr_S it undergoes a pitchfork bifurcation and two subcritical branches of solutions emerge for $Gr < Gr_S$. Neither solution is symmetric, but at a fixed Gr, each is transformed into the other by the symmetry S. These two unstable branches of mixed modes terminate at a (second) primary bifurcation that takes place at $Gr_P \approx 1001.8 > Gr_T$.

When $A = 2.3$ the first primary bifurcation is a pitchfork at $Gr_P \approx 812.4$ where two subcritical unstable branches are created (Fig. 11(b)). With decreasing Gr, these branches of mixed modes approach one another and terminate at a secondary bifurcation point Gr_S, $797.7 < Gr_S < 798.0$. This point is located on the subcritical branch created at the second primary bifurcation at $Gr_T \approx 838$. This branch is twice unstable down to Gr_S below which it is only once unstable. The branch acquires stability at a saddle-node bifurcation at $Gr_{SN} \approx 475$ and remains stable at least up to $Gr = 1000$ (the end of our computational domain). The supercritical branch emerging at Gr_T has one unstable eigenvalue and remains unstable at least up to $Gr = 1000$. For comparison $Gr_{SN} = 676$ when $A = 1$, and $Gr_{SN} = 502$ when $A = 2.6$.

Note that the location of the secondary pitchfork bifurcation switches from the supercritical transcritical branch to the subcritical one as A increases to A_c.

8. Imperfect bifurcation

In this Section, we focus on the influence of a small deviation from the special case $N = -1$ and investigate the two cases $N = -1.01$ and $N = -0.99$ in a square cavity ($A = 1$). The Prandtl number and the Schmidt numbers

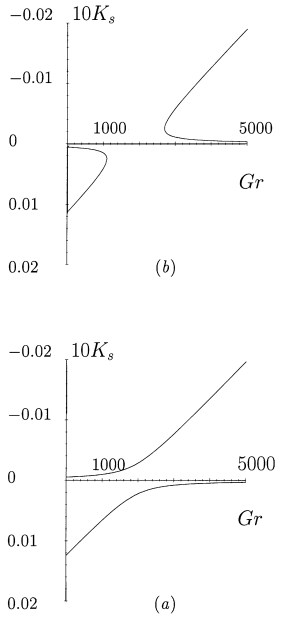

Fig. 12. The amplitude K_s from Eq. (68) with $Gr^{(1)} \equiv Gr - Gr^{(0)}$ as a function of Gr for $Pr = 1$, $Sc = 11$ and (a) $\epsilon' = -0.1$, (b) $\epsilon' = 0.1$.

are fixed at $Pr = 1$ and $Sc = 11$. For this aspect ratio the first bifurcation is transcritical and we therefore focus primarily on the effects of departures from $N = -1$ on this bifurcation. The main effect of this perturbation is the destruction of the trivial equilibrium. It is important to note, however, that the departure of N from -1 does *not* break the symmetry S, i.e., rotation by π around the center of the cavity remains a symmetry of the system (2)–(5). As a result, the pitchfork bifurcations will remain, although they will be shifted to new locations.

8.1. Analytical approach

When $N \neq -1$ the primary bifurcation becomes imperfect since the conduction state is no longer a solution of the equations. Locally, the resulting bifurcation is completely described by adding a small constant ϵ' to the amplitude equation (27):

$$\frac{\partial K_s}{\partial t^{(1)}} = V\,(Gr - Gr_c, K_s) \equiv \frac{K_s(Gr^{(1)}|Pr - Sc| + K_s(b + (Pr + Sc)c))}{(d + (Pr + Sc)e)} + \epsilon'. \tag{68}$$

Here $Gr^{(1)} \equiv Gr - Gr^{(0)}$. Stationary solutions $K_s(Gr)$ for a square cavity are shown in Fig. 12 for $Pr = 1$ and $Sc = 11$ in the two cases: (a) $\epsilon' < 0$ or (b) $\epsilon' > 0$.

8.2. Numerical study

Although the above analytical approach provides the correct local unfolding of the transcritical bifurcation when $N \neq -1$ it is helpful to compare its predictions with numerically computed bifurcation diagrams. Such diagrams for a square container and $N = -1.01$ and $N = -0.99$ are shown in Figs. 13 and 14, respectively. Comparison with Eq. (68) shows that $N = -0.99$ corresponds to $\epsilon' > 0$ while $N = -1.01$ corresponds to $\epsilon' < 0$. Fig. 13 shows that when $N = -1.01$ convection develops continuously as Gr increases and that its sense is counterclockwise ($Le > 1$). This is as expected: when $N = -1.01$, $\Delta C = 1.01|\beta_T/\beta_C|\Delta T$, i.e., the concentration on the left boundary is

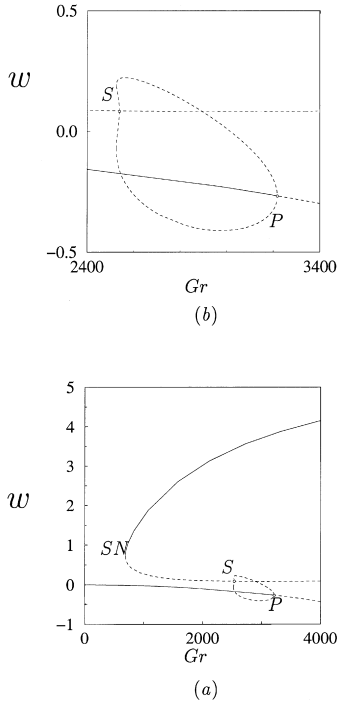

Fig. 13. (a) The vertical velocity $w(0.388, 0.5)$ in a square container with $N = -1.01$ as a function of the Grashof number Gr. (b) Enlargement of (a). The resolution is 15×15. Stable (unstable) solutions are indicated by continuous (dashed) lines. Positive w implies clockwise circulation.

higher than when $N = -1$. Consequently the fluid near the boundary is heavier and therefore sinks setting up a counterclockwise circulation. This circulation is present at all Grashof numbers and its strength increases with Gr. This conclusion agrees with that for $N = -1$ in Section 4.1, viz. that the circulation on the supercritical branch is counterclockwise. Conversely, when $N = -0.99$ the concentration deficit at the left boundary drives a clockwise circulation and this results (see Fig. 14) in a continuous connection between this circulation and the clockwise flow near the original saddle-node bifurcation found in Fig. 11. There is no longer a primary transcritical bifurcation (in comparison with the case $N = -1$) and the secondary pitchfork bifurcation then becomes a first primary pitchfork.

Note that if a similar calculation were done for $A = 1.8$ (see Fig. 11) and N only slightly greater than -1 there would be a *disconnected* interval of *stable* counterclockwise solutions in the lower right, instead of the unstable

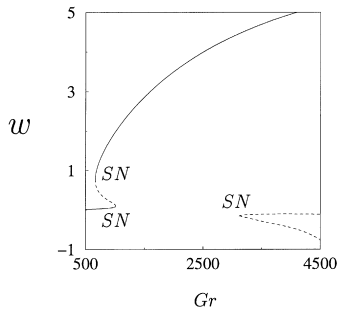

Fig. 14. The vertical velocity $w(0.388, 0.5)$ in a square container with $N = -0.99$ as a function of the Grashof number Gr. The resolution is 15×15. Stable (unstable) solutions are indicated by continuous (dashed) lines. Positive w implies clockwise circulation.

branch seen in Fig. 14. On the left these solutions terminate at the saddle-node bifurcation, while on the right they lose stability at a (subcritical) pitchfork bifurcation that creates a branch of unstable mixed modes that connects to another pitchfork on the other side of the saddle-node. With decreasing $\epsilon' < 0$ or decreasing $A < A_c$ these two pitchfork bifurcations coalesce at the saddle-node bifurcation eliminating the disconnected stable counterclockwise solutions. Thereafter, the only stable states are clockwise ones, and these exhibit hysteresis if $|\epsilon'|$ is not too large as in Fig. 14. Such bifurcation diagrams are found in the unfolding

$$\dot{r} = \epsilon r + arz + \mathcal{O}(3), \quad \dot{z} = \epsilon' + \delta z + br^2 - z^2 + \mathcal{O}(3), \tag{69}$$

corresponding to Eqs. (59). When $ab > 0$ (our case) no additional transitions take place near $(\epsilon, \delta, \epsilon') = (0, 0, 0)$.

9. Conclusion

In this paper we have investigated in some detail the nonlinear states in doubly diffusive convection in a rectangular cavity driven by lateral temperature and concentration differences. Unlike natural convection this configuration does admit, under appropriate conditions, a static equilibrium. We have used this fact to understand the properties of nearby configurations, i.e., configurations that do not admit a trivial solution and which resemble instead natural convection. When $A = 1$ two possibilities were uncovered. In the first, arising when $N < -1$, the strength of convection increases continuously with increasing Grashof number and the circulation is counterclockwise. For sufficiently large Grashof numbers finite amplitude perturbations exist which result in finite amplitude clockwise convection. The counterclockwise state may also lose stability at a pitchfork bifurcation (see Fig. 13) resulting in a hysteretic transition to the clockwise state. When $0 > N > -1$ the situation is more interesting because the small amplitude clockwise circulation that develops with increasing Grashof number loses stability at a finite Grashof number resulting in a hysteretic transition to large amplitude clockwise convection (see Fig. 14). After a gap in Gr a smaller amplitude counterclockwise state may acquire stability, resulting once again in bistability between states of opposite circulation. For typical parameter values our calculations indicate, however, that this counterclockwise state is in fact everywhere unstable so that bistability will not be present. These results were obtained semi-analytically by focusing on the neighborhood of a special aspect ratio at which the static equilibrium loses stability simultaneously to symmetric and antisymmetric modes, and by numerical continuation for other aspect ratios. The results shed substantial light on the mechanism by which multiple stable states arise. However, the restriction $|N + 1| \ll 1$ imposed on the basic state precludes a direct comparison with existing experimental and numerical results for which $|N| > 3$ [12,15,16]. Interestingly, for realistic values of the remaining parameters no Hopf bifurcations were located, and no time-dependence is therefore expected when the basic flow consists of a weak circulation and the Grashof number remains moderate.

Appendix A. Weakly nonlinear analysis

In this section we summarize the multiple scale analysis used to compute the normal forms (27) and (32).

A.1. The symmetric case

Near the onset of the primary instability to a symmetric mode we employ the following expansion in powers of a small parameter $\varepsilon > 0$:

$$\psi' = \varepsilon\psi^{(1)} + \varepsilon^2\psi^{(2)} + \cdots, \tag{A.1}$$

$$T' = \varepsilon T^{(1)} + \varepsilon^2 T^{(2)} + \cdots, \tag{A.2}$$

$$C' = \varepsilon C^{(1)} + \varepsilon^2 C^{(2)} + \cdots, \tag{A.3}$$

$$\frac{\partial}{\partial t} = \varepsilon \frac{\partial}{\partial t^{(1)}} + \varepsilon^2 \frac{\partial}{\partial t^{(2)}} + \cdots, \tag{A.4}$$

$$Gr = Gr^{(0)} + \varepsilon Gr^{(1)} + \varepsilon^2 Gr^{(2)} + \cdots. \tag{A.5}$$

At order ε we recover the eigenvalue problem. The lowest critical Grashof number satisfying the characteristic equation is

$$Gr^{(0)}\,|Sc - Pr| = Gr_c\,|Sc - Pr| = Ra_c\,|Le - 1| = f(A) \text{ or } g(A), \tag{A.6}$$

depending on the mode parity. Noting that $C^{(1)} = Le\,T^{(1)}$, the critical eigenmode can be written in the form

$$\begin{pmatrix} \psi^{(1)} \\ T^{(1)} \\ C^{(1)} \end{pmatrix} = K_s(t^{(1)}) \begin{pmatrix} f_1(x,z) \\ Pr\ f_2(x,z) \\ Sc\ f_2(x,z) \end{pmatrix}, \tag{A.7}$$

where the amplitude K_s depends on the slow time $t^{(1)}$ and the functions f_i ($i = 1$ or 2) depend only on the spatial variables. These functions are computed using the Galerkin method. Interchanging Sc and Pr changes $f_1(x,z)$ into $-f_1(x, A-z)$ and $f_2(x,z)$ into $f_2(x, A-z)$.

At order ε^2 the equations are:

$$\begin{aligned} &\begin{pmatrix} \Delta^2 & Gr^{(0)}(\partial/\partial x) & -Gr^{(0)}(\partial/\partial x) \\ -\partial/\partial z & \Delta/Pr & 0 \\ -\partial/\partial z & 0 & \Delta/Sc \end{pmatrix} \begin{pmatrix} \psi^{(2)} \\ T^{(2)} \\ C^{(2)} \end{pmatrix} \\ &\quad = -\begin{pmatrix} 0 & Gr^{(1)}(\partial/\partial x) & -Gr^{(1)}(\partial/\partial x) \\ 0 & 0 & 0 \\ 0 & 0 & 0 \end{pmatrix} \begin{pmatrix} \psi^{(1)} \\ T^{(1)} \\ C^{(1)} \end{pmatrix} - \begin{pmatrix} N_1(\psi^{(1)}, \psi^{(1)}) \\ N_2(\psi^{(1)}, T^{(1)}) \\ N_2(\psi^{(1)}, C^{(1)}) \end{pmatrix} + \frac{\partial}{\partial t^{(1)}} \begin{pmatrix} \Delta\psi^{(1)} \\ T^{(1)} \\ C^{(1)} \end{pmatrix}. \end{aligned} \tag{A.8}$$

The existence of a convective solution requires the solvability lemma [42] to be satisfied, i.e., there must exist a non-zero solution to the following adjoint linear eigenvalue problem:

$$\begin{pmatrix} \Delta^2 & \partial/\partial z & \partial/\partial z \\ -Gr^{*(0)}(\partial/\partial x) & \Delta/Pr & 0 \\ Gr^{*(0)}(\partial/\partial x) & 0 & \Delta/Sc \end{pmatrix} \begin{pmatrix} \psi^* \\ T^* \\ C^* \end{pmatrix} = \begin{pmatrix} 0 \\ 0 \\ 0 \end{pmatrix} \tag{A.9}$$

with identical boundary conditions. This condition yields the result

$$Gr^{*(0)}|Sc - Pr| = f(A) \text{ or } g(A), \tag{A.10}$$

the corresponding non-zero solution is

$$\begin{pmatrix} \psi^* \\ T^* \\ C^* \end{pmatrix} = \begin{pmatrix} (Pr - Sc) f_1^*(x,z) \\ Pr\ f_2^*(x,z) \\ -Sc\ f_2^*(x,z) \end{pmatrix}. \tag{A.11}$$

The amplitude equation (27) now follows on applying the Fredholm alternative.

A.2. The antisymmetric case

In this case the quadratic terms necessarily vanish and we can set $Gr^{(1)} = 0$ and omit the timescale $t^{(1)}$.

In order to obtain the first non-zero $Gr^{(i)}$ for $i = \{1, 2, 3, \ldots, n\}$, we solve the order ε^2 problem for $\psi^{(2)}$, $T^{(2)}$ and $C^{(2)}$. We find:

$$\begin{pmatrix} \psi^{(2)} \\ T^{(2)} \\ C^{(2)} \end{pmatrix} = K_a^2(t^{(2)}) \begin{pmatrix} g_1(x, z, Pr, Sc) \\ g_2(x, z, Pr, Sc) \\ g_3(x, z, Pr, Sc) \end{pmatrix}. \tag{A.12}$$

At order ε^3, we obtain

$$\begin{aligned} &\begin{pmatrix} \Delta^2 & Gr^{(0)}(\partial/\partial x) & -Gr^{(0)}(\partial/\partial x) \\ -\partial/\partial z & \Delta/Pr & 0 \\ -\partial/\partial z & 0 & \Delta/Sc \end{pmatrix} \begin{pmatrix} \psi^{(3)} \\ T^{(3)} \\ C^{(3)} \end{pmatrix} \\ &\quad = -\begin{pmatrix} 0 & Gr^{(2)}(\partial/\partial x) & -Gr^{(2)}(\partial/\partial x) \\ 0 & 0 & 0 \\ 0 & 0 & 0 \end{pmatrix} \begin{pmatrix} \psi^{(2)} \\ T^{(2)} \\ C^{(2)} \end{pmatrix} - \begin{pmatrix} N_1(\psi^{(1)}, \psi^{(2)}) \\ N_2(\psi^{(1)}, T^{(2)}) \\ N_2(\psi^{(1)}, C^{(2)}) \end{pmatrix} - \begin{pmatrix} N_1(\psi^{(2)}, \psi^{(1)}) \\ N_2(\psi^{(2)}, T^{(1)}) \\ N_2(\psi^{(2)}, C^{(1)}) \end{pmatrix} \\ &\qquad + \frac{\partial}{\partial t^{(2)}} \begin{pmatrix} \Delta\psi^{(1)} \\ T^{(1)} \\ C^{(1)} \end{pmatrix}. \end{aligned} \tag{A.13}$$

The Fredholm alternative now yields the result (32).

General theory [32] shows that the above normal forms need not be arbitrarily truncated at second and third order, respectively; instead all higher order terms can be transformed away by near-identity transformations, provided the non-degeneracy conditions stated in Section 4 hold. This is the case here.

References

[1] J.S. Turner, Double diffusive phenomena, Annu. Rev. Fluid Mech. 6 (1974) 37–56.
[2] J.S. Turner, Buoyancy Effects in Fluids, Cambridge University Press, Cambridge, 1979.
[3] J.S. Turner, Multicomponent convection, Annu. Rev. Fluid Mech. 17 (1985) 11–44.
[4] W.R. Wilcox, Transport phenomena in crystal growth from solution, Prog. Crystal Growth Charact. 26 (1993) 153–194.
[5] E. Knobloch, D.R. Moore, J. Toomre, N.O. Weiss, Transitions to chaos in two-dimensional double-diffusive convection, J. Fluid Mech. 166 (1986) 409–448.
[6] G. Veronis, Effect of a stabilizing gradient of solute on thermal convection, J. Fluid Mech. 34 (1968) 1–17.
[7] D.R. Moore, N.O. Weiss, Dynamics of double convection, Phil. Trans. R. Soc. London A 332 (1990) 121.
[8] N. Tsitverblit, E. Kit, The multiplicity of steady flows in confined double-diffusive convection with lateral heating, Phys. Fluids A 5 (1993) 1062–1064.
[9] N. Tsitverblit, Bifurcation phenomena in confined thermosolutal convection with lateral heating: commencement of the double-diffusive region, Phys. Fluids 7 (1995) 718–736.
[10] E.J. Kranenborg, H.A. Dijkstra, The structure of (linearly) stable double diffusive flow patterns in a laterally heated stratified liquid, Phys. Fluids 7 (1995) 680–682.
[11] L.W. Wang, Y. Kamotani, S. Ostrach, Experimental study of natural convection in a shallow horizontal cavity with different end temperatures and concentrations, Report FATS/TR-81-164, Case Western University, 1983.
[12] Y. Kamotani, L.W. Wang, S. Ostrach, H.D. Jiang, Experimental study of natural convection in shallow enclosures with horizontal temperature and concentration gradients, Int. J. Heat Mass Transfer 28 (1985) 165–173.
[13] H.D. Jiang, S. Ostrach, Y. Kamotani, Thermosolutal convection with opposed buoyancy forces in shallow enclosures, in: R.S. Figliola, P.G. Simpkins (Eds.), Natural Convection in Enclosures — 1988, Natural Convection in Enclosures ASME HTD 28 (1988) 165.

[14] H.D. Jiang, S. Ostrach, Y. Kamotani, Unsteady thermosolutal transport phenomena due to opposed buoyancy forces in shallow enclosures, J. Heat Transfer 113 (1991) 135–140.
[15] J. Lee, M.T. Hyun, K.W. Kim, Natural convection in confined fluids with combined horizontal temperature and concentration gradients, Int. J. Heat Mass Transfer 31 (1988) 1969–1977.
[16] J.W. Lee, J.M. Hyun, Double-diffusive convection in a rectangle with opposing horizontal temperature and concentration gradients, Int. J. Heat Mass Transfer 33 (1990) 1619–1632.
[17] J.M. Hyun, J.W. Lee, Double-diffusive convection in rectangle with cooperating horizontal gradients of temperature and concentration, Int. J. Heat Mass Transfer 33 (1990) 1605–1617.
[18] R. Bennacer, D. Gobin, Cooperating thermosolutal convection in enclosures —I. Scale analysis and mass transfer, Int. J. Heat Mass Transfer 39 (1996) 2671–2681.
[19] D. Gobin, R. Bennacer, Cooperating thermosolutal convection in enclosures —II. Heat transfer and flow structure, Int. J. Heat Mass Transfer 39 (1996) 2683–2697.
[20] W.J. Chang, H.C. Lin, Natural convection in a finite wall rectangular cavity filled with an anisotropic porous medium, Int. J. Heat Mass Transfer 37 (1994) 303–312.
[21] F. Alavyoon, On natural convection in vertical porous enclosures due to opposing fluxes of heat and mass prescribed at the vertical walls, Int. J. Heat Mass Transfer 36 (1993) 2479–2498.
[22] K. Ghorayeb, A. Mojtabi, Double diffusive convection in a vertical rectangular cavity, Phys. Fluids 9 (1997) 2339–2348.
[23] S. Xin, P. Le Quéré, L.S. Tuckerman, Bifurcation analysis of double-diffusive convection with opposing horizontal thermal and solutal gradients, Phys. Fluids 10 (1998) 850–858.
[24] A. Bergeon, K. Ghorayeb, A. Mojtabi, Double diffusive instability in an inclined box, Phys. Fluids 11 (1999) 549–559.
[25] E. Knobloch, Convection in binary fluids, Phys. Fluids 23 (1980) 1918–1920.
[26] J.D. Crawford, E. Knobloch, Symmetry and symmetry-breaking bifurcations in fluid dynamics, Annu. Rev. Fluid Mech. 23 (1991) 341–387.
[27] D. Henry, B. Roux, Soret separation in a quasi-vertical cylinder, J. Fluid Mech. 195 (1988) 175–200.
[28] D.S. Riley, K.H. Winters, Modal exchange in Lapwood convection, J. Fluid Mech. 204 (1989) 325–358.
[29] K.H. Winters, T.H. Plesser, K.A. Cliffe, The onset of convection in a finite container due to surface tension and buoyancy, Physica D 29 (1989) 387–401.
[30] P. Hirschberg, E. Knobloch, Mode interaction in large aspect ratio convection, J. Nonlinear Sci. 7 (1997) 537–556.
[31] J. Guckenheimer, P. Holmes, Nonlinear Oscillations, Dynamical Systems and Bifurcations of Vector Fields, Springer, New York, 1986.
[32] M. Golubitsky, D.G. Schaeffer, Singularities and Groups in Bifurcation Theory, vol. 1, Springer, New York, 1985.
[33] B. Straughan, The Energy Method, Stability, and Nonlinear Convection, Springer, New York, 1992, pp. 38–105.
[34] W.F. Langford, Periodic and steady-state mode interactions lead to tori, SIAM J. Appl. Math. 37 (1979) 22–48.
[35] R.W. Wittenberg, P. Holmes, The limited effectiveness of normal forms: a critical review and extension of local bifurcation studies of the Brusselator PDE, Physica D 100 (1997) 1–40.
[36] A.T. Patera, A spectral element method for fluid dynamics: laminar flow in a channel expansion, J. Comput. Phys. 54 (1984) 468–488.
[37] G.Em. Karniadakis, M. Israeli, S.A. Orszag, High-order splitting method for the incompressible Navier–Stokes equations, J. Comput. Phys. 97 (1991) 414–443.
[38] L.S. Tuckerman, Steady-state solving via Stokes preconditioning: recursion relations for elliptic operators, in: D.L. Dwoyer, M.Y. Hussaini, R.G. Voigt (Eds.), Proceedings of the 11th International Conference on Numerical Methods in Fluid Dynamics, Springer, New York, 1989.
[39] C.K. Mamun, L.S. Tuckerman, Asymmetry and Hopf bifurcation in spherical Couette flow, Phys. Fluids 7 (1995) 80–91.
[40] A. Bergeon, Instabilité de Marangoni–Bénard en présence d'effet Soret, Ph.D. Thesis, Ecole Centrale de Lyon, 1995.
[41] A. Bergeon, D. Henry, H. BenHadid, L.S. Tuckerman, Marangoni convection in binary mixtures with Soret effect, J. Fluid Mech. 375 (1998) 143–177.
[42] D.D. Joseph, D.H. Sattinger, Bifurcating time periodic solutions and their stability, Arch. Rational Mech. 69 (1972) 79.